Discover Materials

Research

Strategic enhancement of joint strength in dissimilar Al/Mg alloys: a workable approach for aerospace application

S. Suresh[1] · Elango Natarajan[2] · Kalaimani Markandan[2] · S. Sudhagar[3] · Gnanasambandam Anbuchezhiyan[4] · R. Elayaraja[5]

Received: 31 August 2024 / Accepted: 13 January 2025
Published online: 05 February 2025

Abstract
The increasing importance of dissimilar lightweight metal joints is crucial for advancing aerospace and automotive technologies, where aluminum (Al) and magnesium (Mg) alloys offer an ideal balance of strength and weight. However, the challenges associated with joining these dissimilar metals necessitate innovative solutions. This study explores the role of silicon carbide (SiC) nanoparticles in enhancing the friction stir spot welding (FSSW) of dissimilar alloys AA6061 and AZ31B. The methodology involved varying the rotational speed of the welding tool (1000, 1200, 1400, and 1600 rpm) while keeping other parameters such as plunge depth, plunge rate, and dwell time constant. SiC nanoparticles were introduced through a pre-drilled 2 mm hole at the tool's plunging point to refine the microstructure and mitigate the formation of brittle Al–Mg intermetallic compounds (IMCs). The addition of SiC nanoparticles modifies the weld microstructure, reducing the formation of brittle Al–Mg IMCs and promoting the development of finer, well-distributed Mg–SiC IMCs, resulting in a more favorable and homogeneous multilayered structure. The incorporation of SiC significantly enhances the strength of the joints, achieving a maximum of 5.68 kN, 22.7% increase compared to SiC-free Al/Mg joints. This improvement underscores potentiality of SiC as a reinforcing element in strengthening dissimilar metal joints and demonstrates the effectiveness of it in dissimilar Al/Mg joints, making them suitable for aerospace and automotive applications.

Keywords Aluminum (Al) · Magnesium (Mg) · Alloys · SiC · Intermetallic compounds · Sustainable manufacturing

1 Introduction

Lightweight alloys such as aluminium, magnesium, titanium and copper are potential engineering alloys from research and industrial point of view. These alloys have become more significant in the transport manufacturing industries, including aircraft, cars, heavy trucks, trains, ships, and defence products [1–3]. These alloys are appealing for steel structures in some engineering applications due to their characteristics such as a high strength-to-weight ratio, effective heat conductivity, and excellent damping capacity [4–6].

✉ Elango Natarajan, elango@ucsiuniversity.edu.my; S. Suresh, suresh.mjl@gmail.com | [1]Department of Mechanical Engineering, Erode Sengunthar Engineering College, Erode, Tamilnadu, India. [2]Faculty of Engineering, Technology and Built Environment, UCSI University, Kuala Lumpur, Malaysia. [3]Department of Mechanical Engineering, Kalaignarkarunanidhi Institute of Technology, Coimbatore, Tamilnadu, India. [4]Department of Mechanical Engineering, Saveetha School of Engineering, Saveetha Institute of Medical and Technical Sciences, Saveetha University, Chennai, Tamilnadu, India. [5]School of Mechanical Engineering, Vellore Institute of Technology, Vellore, Tamilnadu, India.

Aluminum (Al) and magnesium (Mg) alloys are widely utilized in the aerospace, automotive, and defense industries due to their lightweight properties, high specific strength, and excellent corrosion resistance. The combination of these alloys offers a promising solution for applications where weight reduction is essential without compromising performance [7]. In the aerospace sector, Al/Mg alloys are employed for internal structural frames, panels, and fuselages to reduce overall aircraft weight, leading to improved fuel efficiency and higher payload capacity. Components such as gearbox housings and rotor supports further benefit from the high strength-to-weight ratio of these joints, enhancing flight dynamics by reducing inertia. The aerospace industry among others, increasingly demands the joining of dissimilar materials to achieve benefits such as cost efficiency, design flexibility, and significant weight reduction [8–10]. Whereas, fusion welding processes such as shielded metal arc welding, gas metal arc welding, and gas tungsten arc welding lead to metallurgical mismatching in the weld dissimilar materials in metal-to-metal joints [11, 12]. Friction Stir Welding (FSW) and Friction Stir Spot Welding (FSSW) have emerged as promising techniques for producing high-quality joints in various dissimilar alloy systems, particularly when the metals involved possess distinct physical or mechanical properties [13]. In FSW, the significant process parameters include tool rotation speed, tool traverse speed, and tool plunge force [14, 15]. These parameters play a crucial role in determining the quality and strength of the weld. The FSSW process operates on a similar principle but differs in that the tool does not travel linearly. Instead, FSSW involves plunging, stirring, and retracting, making it particularly suitable for spot-joining applications [16, 17]. Unlike conventional welding processes that involve melting, FSW/FSSW achieves coalescence through localized heat generated by the stirring action of a non-consumable rotating tool, applied with modest clamping force [18, 19]. These solid-state processes offer a viable alternative to conventional fusion welding methods, which often struggle with or fail to effectively join materials with sharply differing characteristics, such as Al alloys to Mg alloys or Al alloys to steel.

While the application of FSW/FSSW to dissimilar materials presents challenges especially when dealing with combinations that exhibit stark contrasts in their properties the techniques have already been successfully employed in the mass production of automotive structural components, specifically for Al-alloy to steel joints. Expanding the use of FSW/FSSW to more complex material combinations, such as Al alloys to Mg alloys or Mg alloys to steel, holds the potential for even greater weight reductions and enhanced performance in aerospace and other high-performance applications. The incorporation of nanoparticles, such as SiC, Al_2O_3 [20, 21] and Fe_2O_3 [22] can further improve the mechanical properties of welded joints by promoting grain refinement and enhancing interfacial bonding [23–25]. This advancement could help overcome some of the inherent challenges of joining similar and dissimilar materials, leading to joints with superior strength and durability [26–28].

In recent years, various studies have explored the use of FSW/FSSW for joining different combinations of aluminum and magnesium alloys. Brittle intermetallic compounds (IMCs) make it difficult to produce strong Al/Mg joints [29, 30]. Addressing this issue is paramount, especially given the increasing demand for lightweight and high-performance materials in contemporary engineering applications. In the context of solid-state joining techniques like FSSW, the formation of $Mg_{17}Al_{12}$ and Al_3Mg_2 IMCs poses inherent challenges. These compounds, even in trace amounts, can significantly impact the structural integrity and performance of the joints [31, 32].

Research by Zhibo et al. [33] focused on the impact of varying the joining time on the formation of intermetallic compounds and the filling characteristics in FSSW of Al/AZ31B alloy joints. They found that extending the joining time led to the development of a thicker intermetallic layer, which initially increased the joint strength. However, as the intermetallic layer continued to thicken, the joint strength eventually peaked and then began to decrease. Studies have shown that the introduction of a thin intermetallic compound layer of $Al_{12}Mg_{17}$ during refill friction stir spot welding (RFSSW) of aluminum-magnesium alloys significantly increases the hardness of the joint. This method has led to superior static shear strength compared to traditional spot friction welds, which is critical for improving the joint's mechanical properties [34]. Chowdhury et al. [35] explored the fatigue and shear strength of FSS welded dissimilar joints between Al and mg alloys. They examined three configurations: Al on top of Mg, Al on Mg with an adhesive interlayer, and Mg on Al with an adhesive interlayer. Across all configurations, the stir zone (SZ) was found to contain intermetallic compounds such as Al_3Mg_2 and $Al_{12}Mg_{17}$, which contributed to increased hardness [36]. Wu et al. [37] employed swing friction stir spot welding (S-FSSW) to join aluminum and magnesium alloys, comparing this technique with conventional friction stir spot welding (C-FSSW). Their study revealed that in S-FSSW joints, the intermetallic compound (IMC) structure at the interface exhibited a spherical morphology, contrasting with the dendritic structure typically observed in conventional FSSW joints.

Recently, many researchers developed a new lightweight metal that welded through FSW/FSSW with the addition of ceramic nanoparticles that regarded as super-strong yet high-performance lightweight metals [38–43]. They reported the use of nanoparticles in the FSW/FSSW process, composite matrix, and the implication of these process method on

Table 1 Chemical composition (% weight) of AA6061-T6 and AZ31-B

Base material	Elements					
	Cu	Mn	Al	Si	Fe	Mg
AA6061-T6	0.05	0.2	2.5	–	0.1	0.005
AZ31-B	0.35	0.15	95.8	0.5	0.7	0.8

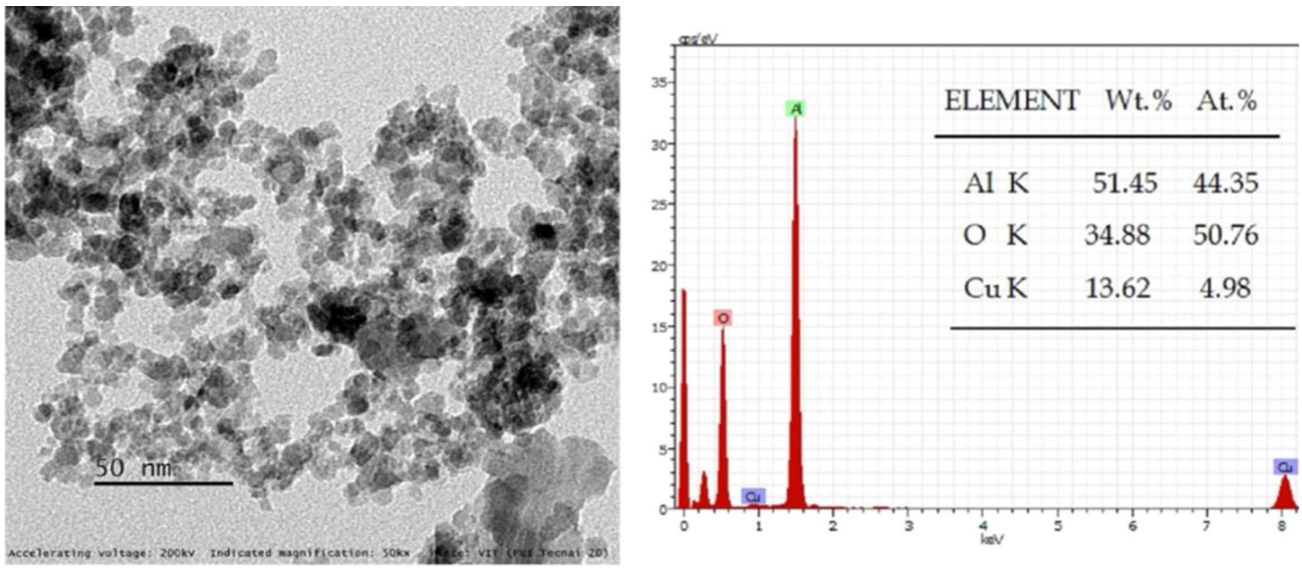

Fig. 1 TEM–EDX of as received SiC nanoparticles

mechanical properties [44–46]. Based on the previous discussions, it is noticeable that many studies paid attention on investigating different process parameters for joining Al and Mg dissimilar materials through FSW/FSSW.

Despite the growing interest in the FSSW of Al and Mg alloys, there is still limited information in the open literature regarding the incorporation of nanoparticles and its effect on weld characteristics. At this end, the present study aims to explore the impact of SiC nanoparticle reinforcement on the mechanical strength and microstructures of FSSW of aluminium alloy 6061-T6 and AZ31-B magnesium alloys. On top of it, it is to derive and report methodology of uniform particle dispersion, optimization of process parameters and effect of varying tool rotational speeds to achieve defect-free joints.

2 Materials and methods

The welding specimens were prepared using 6061-T6 aluminum alloy and AZ31-B magnesium alloy plates of 2 mm thickness, obtained from Cluster Trading Corporation, India. These plates were cut to size with dimensions of 100 × 35 mm using Electrical Discharge Machining (EDM) with an overlapping area of 35 × 35 mm. The physical properties of these materials are listed in Table 1. Additionally, silicon carbide (SiC) nanoparticles, sized at 50 nm, were used as reinforcement to create composite dissimilar joints. TEM–EDX of as received SiC nanoparticles is shown in Fig. 1. Before welding is started, Mg alloy plate (top sheet) and Al alloy plate (bottom sheet) were positioned and SiC nanoparticles were packed into 2 mm diameter pre-drilled hole that appears at the center of the overlapping area (35 × 35 mm) [47–49]. FSSW experiments were carried out using a CNC vertical machining center (ACE Micrometric) equipped with a specialized fixture to securely clamp the overlapping sheets, as shown in Fig. 2a.

The FSSW tool employed was made of H13 steel, hardened to 52–55 HRC. It featured a shoulder diameter of 12 mm, a threaded cylindrical pin of 5 mm diameter, and a length of 2.85 mm. Figure 2a depicts the detailed configuration of the FSSW tool used. A series of preliminary studies and a comprehensive review of the literature informed the range of weld parameters. Four different rotational speeds were tested: 1000, 1200, 1400, and 1600 rpm. To ensure consistency across all tests, the shoulder plunge depth was set as 0.2 mm, the tool travel speed at 10 mm/min, and the dwell time

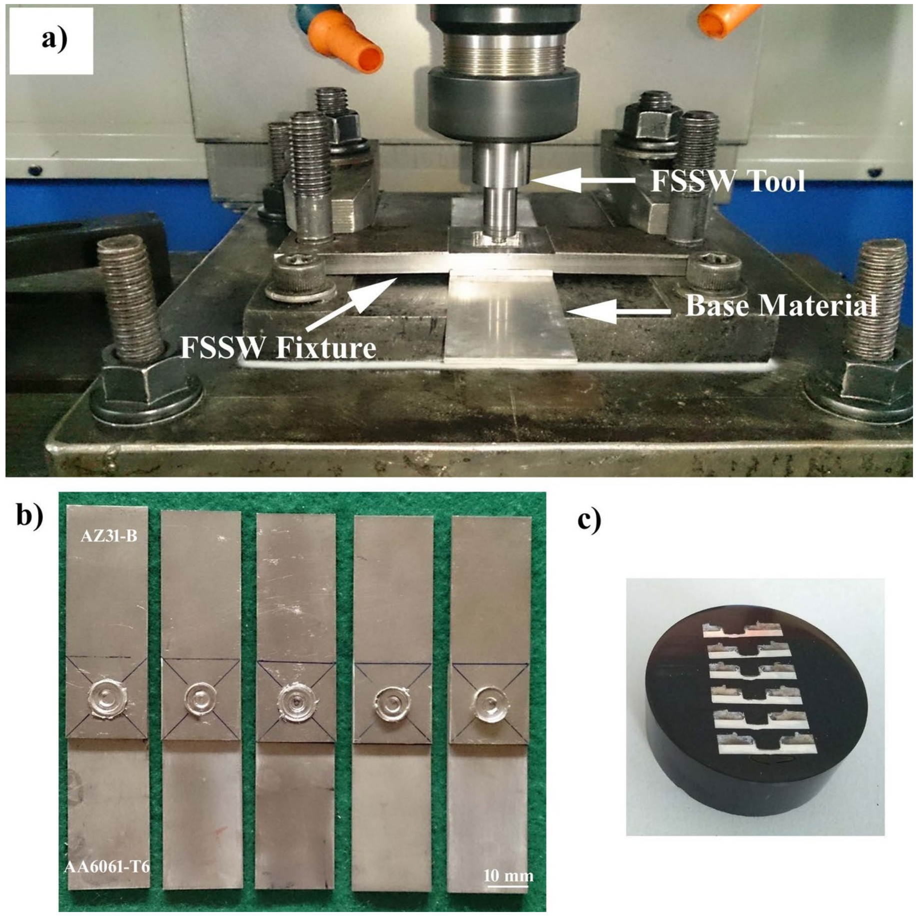

Fig. 2 **a** Experimental setup, **b** fabricated FSSW joint samples and **c** samples used in microstructural examination

at 5 s. Before welding, the overlapping surfaces were meticulously cleaned with acetone to remove any contaminants. Three samples were prepared for each experimental condition to ensure the reproducibility and reliability of the results.

The mechanical properties of the welded joints were evaluated using Vickers microhardness testing (Wilson Hardness, 402 MVD, Wilson Instruments, Norwood) and lap shear strength testing using a computerized universal testing machine (TE-JINAN-WDW100, Jinan Test Machine Co. Ltd, China). Microhardness profiles were recorded at a load of 1 kg and a dwell time of 20 s. Lap shear tests were conducted at room temperature with a crosshead speed of 1 mm/min, and the lap shear strength was calculated as the average of three specimens under each set of welding conditions.

Following the lap shear tests, the welded joints were sectioned and prepared for metallurgical examination using standard metallographic techniques. Keller's reagent, composed of 5 ml HNO_3, 3 ml HCl, 2 ml HF, and 190 ml H_2O, was used to etch the cross-sectional samples and reveal the microstructure. Macrostructural analysis was conducted with a stereo zoom microscope (Radical RSM-9, Radical Scientific, India), while microstructural examination was performed using an optical microscope (Invertoplan TR, Gippon-Japan). The prepared sample for both lap shear testing and metallurgical analysis is illustrated in Fig. 2 (b,c). To further investigate the SZ microstructure and the fracture surfaces of the lap shear-tested specimens were analyzed using a Field Emission Scanning Electron Microscope (FESEM, SIGMA HV—Carl Zeiss, Germany).

3 Results and discussion

3.1 Joint structure

Welded joints were longitudinally sectioned in order to examine their cross-sections visually. Figure 3 shows the cross-sectional images of the Al/Mg/SiC FSSW joints produced at rotational speeds of 1000, 1200, 1400, and 1600 rpm, all defect-free. The study highlights the effectiveness of the FSSW technique in successfully joining dissimilar Al and Mg

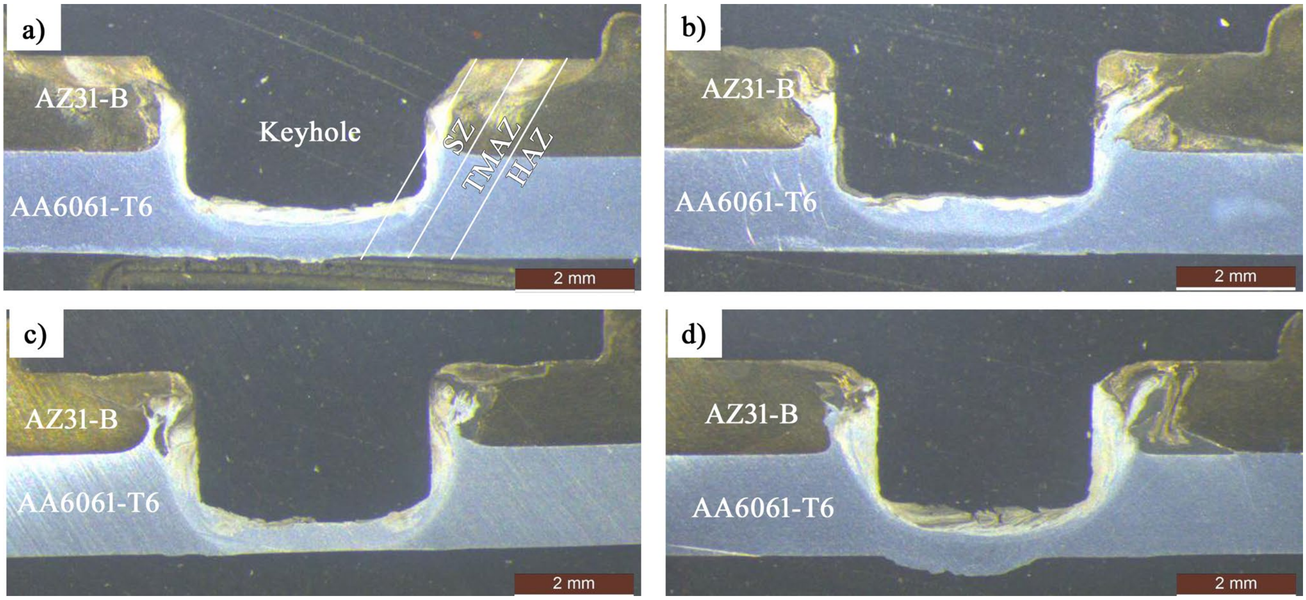

Fig. 3 Cross-sectional macrostructure of welded samples at different tool rotational speeds **a** 1000 rpm, **b** 1200 rpm, **c** 1400 rpm and **d** 1600 rpm

alloys. It is understood that stirring action of the rotating tool pin facilitated plastic flow between the base materials. It could be understood from macroscopic analysis that the distribution of the materials within the weld is significantly influenced by the tool's rotational speed. At lower speeds (1000 rpm, Fig. 3a), the stir zone (SZ) is relatively narrow, and the mixing of Al and Mg remains limited to the keyhole edges. The SZ widens as the speed increases to 1200 and 1400 rpm (Fig. 3b and c), indicating increased material flow that enhanced mixing of Al, Mg, and SiC particles. At these speeds, the Al alloy penetrates upward into the Mg alloy along the keyhole edges, forming a well-defined SZ. This increased intermixing of materials ensures a more homogeneous joint, and contributes to improved mechanical properties. However, as shown in Fig. 3d, the weld produced at 1600 rpm exhibits a broader SZ but with sign of excessive plastic deformation. The excessive heat generated at this speed causes the Al and Mg alloys to mix beyond optimal levels, leading to a coarser grain structure and potential weakening of the joint. At this end, we understand that while the increased stirring improves material flow, it also raises the risk of forming intermetallic compounds (IMCs) such as Al_3Mg_2 and $Al_{12}Mg_{17}$, which may reduce the joint's strength.

Figure 4 presents a comprehensive analysis of the weld SZ structure at a tool rotational speed of 1400 rpm, including microstructure observations across different regions of the joint. The macro image clearly shows the overall shape of the composite weld, with the SZ prominently visible. The SZ, formed through the intense stirring action of the tool, appears defect-free, indicating an effective bond between the Al and Mg alloys. The distinct boundary between the base materials and the SZ suggests good material mixing and a sound metallurgical joint. The micrograph of the mixing zone between Al and Mg reveals a refined grain structure (Refer to Fig. 4b). The fine grains result from dynamic recrystallization during the FSSW process, which is intensified by the presence of SiC nanoparticles [50]. The uniform distribution of these fine grains indicates efficient material flow and mixing at this rotational speed, which is crucial for enhancing the joint's mechanical properties [51, 52].

The microstructure on the Mg side of the joint reveals a blend of equiaxed and elongated grains, with the grain size being larger compared to the mixing zone, as shown in Fig. 4c. This variation in grain size is attributed to the thermal gradient and the relatively lower heat input received on the Mg side during welding, which leads to incomplete dynamic recrystallization. The lower heat input limits the extent of grain refinement, resulting in fewer nucleation sites for new grains. However, the grain refinement achieved is still sufficient to enhance the mechanical properties, particularly in terms of strength and ductility. The Al side of the weld displays a more uniform and refined grain structure compared to the Mg side as shown in Fig. 4d. The smaller grain size is indicative of higher heat input and more intense plastic deformation on the Al side during the FSSW process. This fine-grain structure is beneficial for enhancing the strength of the joint, contributing to the overall integrity and performance of the weld [53, 54].

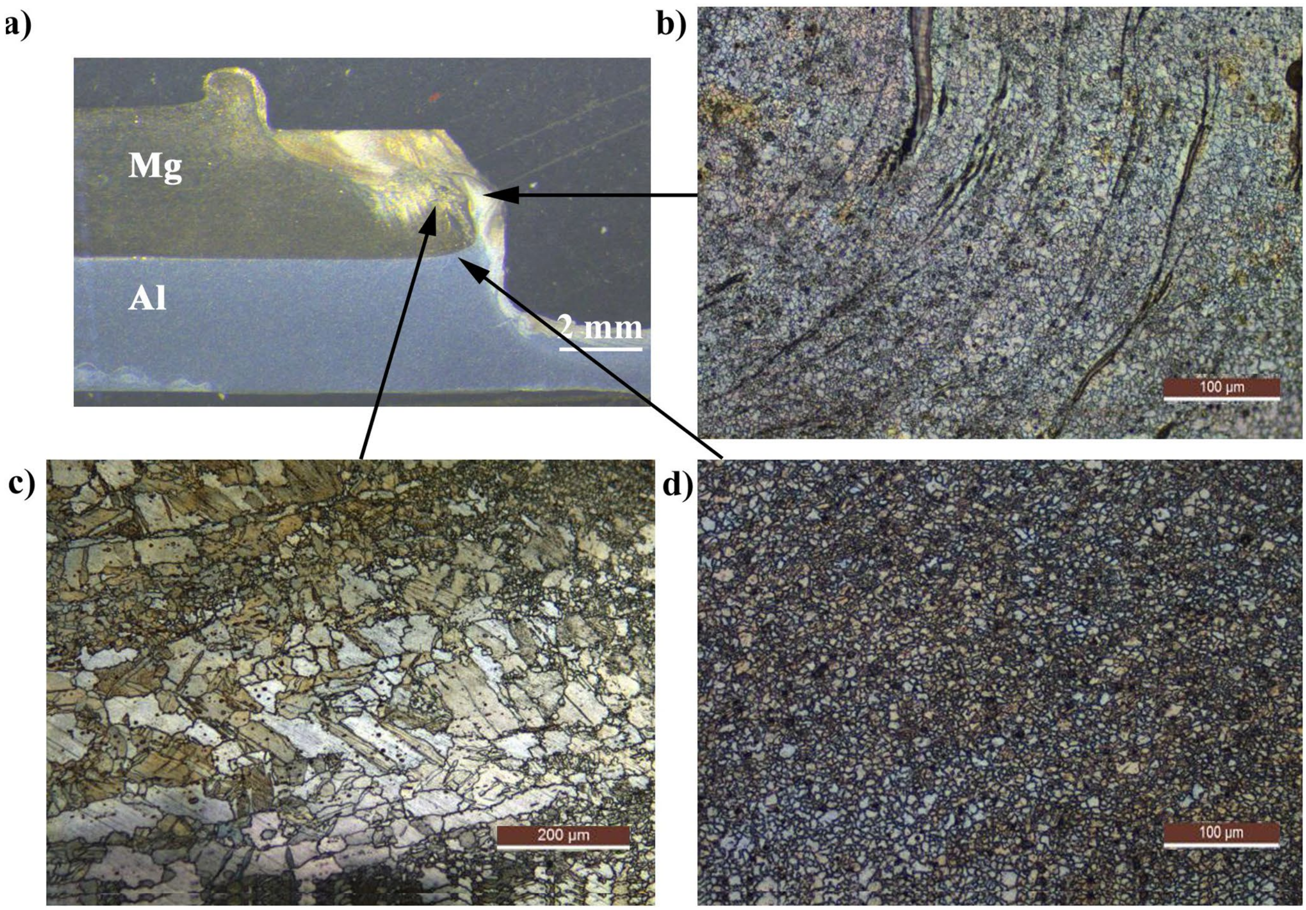

Fig. 4 **a** Macrostructure of the joint at 1200 rpm, **b** SZ microstructure near the interface, **c** Grain structure on the Mg side, and **d** Fine, recrystallized grains in the Al-rich zone

The macrostructure and microstructure analyses of the sample welded at 1600 rpm reveal some critical insights. As shown in Fig. 5, the macrostructure indicates that the weld zone is broader compared to the 1400 rpm sample. However, despite the increased stirring, the higher rotational speed resulted in lower joint strength. This reduction in strength can be attributed to excessive heat generation, which led to improper mixing of the Al and Mg alloys within the SZ [55, 56]. The microstructure analysis further supports this observation. The image in Fig. 5b, showcasing the SZ, reveals a coarser grain structure in the Al/Mg mixture, indicating that the increased heat may have caused grain growth rather than refinement. In contrast to the more refined grains observed at 1400 rpm, the coarse grains at 1600 rpm suggest less effective stirring and intermixing of materials. Figure 5c, showing the microstructure on the Mg side, and Fig. 5d, showing the Al side, both display uneven grain sizes, with some regions indicating partial mixing and others showing a lack of homogeneity. This inconsistency in grain structure reflects the adverse effects of excessive rotational speed on the material's flow and mixing behaviour, leading to a weaker joint.

The FESEM images and EDS analysis at the Al/Mg interface (shown in Fig. 6) provide insights into the formation of IMCs during the FSSW process at different rotational speeds. At 1400 rpm (Fig. 6a), the FESEM and EDS analysis shows a relatively uniform interface between Al and Mg, with the SiC nanoparticles well-distributed within the stir zone. The EDS spectrum indicates the presence of Al, Mg, traces of oxygen (O), SiC. The limited presence of oxygen suggests that there may be minor oxide formation, but it does not dominate the interface. The microstructural refinement seen at this speed suggests that the heat generated was sufficient to allow for good material mixing without excessive intermetallic formation [55]. This controlled environment likely reduces the risk of forming brittle intermetallic phases, which could negatively impact the joint's mechanical properties. The presence of SiC nanoparticles can act as a barrier to the excessive diffusion of Al and Mg atoms, thereby limiting the formation of IMCs [57]. The SiC nanoparticles may also contribute to grain refinement by providing nucleation sites during the recrystallization process as represented in Fig. 7. At 1400 rpm, the microstructural analysis (refer to Fig. 7) showed

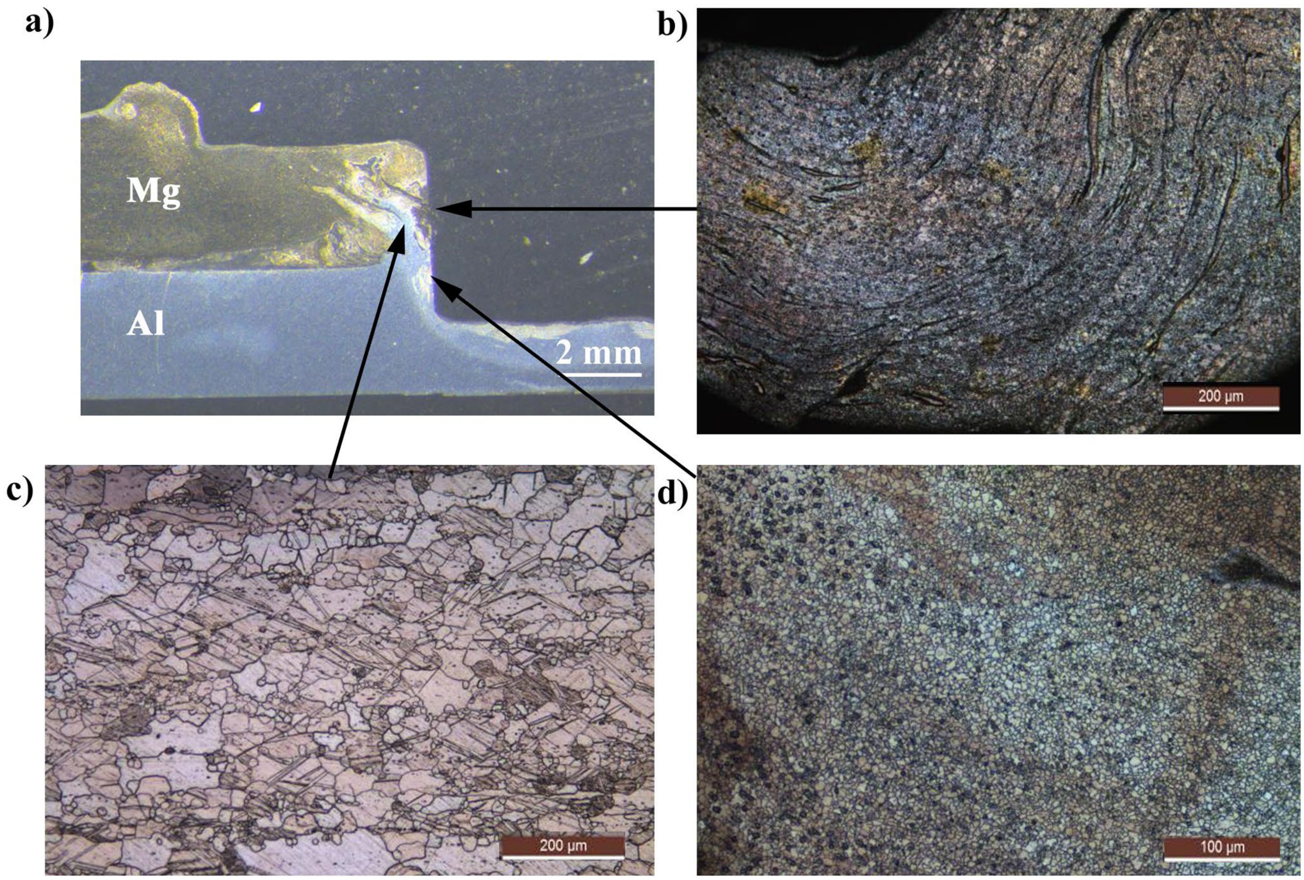

Fig. 5 **a** Macrostructure of the joint at 1600 rpm, **b** SZ microstructure near the interface, **c** Grain structure on the Mg side, and **d** fine, recrystallized grains in the Al-rich zone

a uniform dispersion of SiC nanoparticles throughout the SZ, with minimal signs of agglomeration. The uniform particle distribution was facilitated by efficient stirring and adequate plastic flow of both Al and Mg alloys. This distribution enhanced grain refinement through dynamic recrystallization, leading to improved mechanical properties. The SiC nanoparticles acted as nucleation sites during the recrystallization process, contributing to fine grain structures and limiting the formation of brittle Al–Mg IMCs. This controlled formation of IMCs, coupled with the grain refinement due to SiC, results in a joint with enhanced mechanical properties and reduced brittleness [58, 59]. The findings of this study align with recent works on friction stir welding and additive manufacturing, where SiC particles were used to enhance mechanical properties [60–62].

At 1600 rpm (Fig. 6b), the EDS analysis reveals a more significant presence of intermetallic compounds at the interface. The higher rotational speed leads to increased heat generation, which can promote the diffusion of Al and Mg atoms, enhancing the formation of intermetallic compounds such as Al_3Mg_2 and $Al_{12}Mg_{17}$. The presence of SiC and O in the EDS spectrum indicates potential oxide formation, further contributing to the complexity of the interfacial region. Despite the presence of SiC nanoparticles, which typically help inhibit excessive intermetallic growth, the elevated temperatures at this speed likely override the beneficial effects of SiC. This results in a thicker intermetallic layer, with the SiC nanoparticles potentially getting engulfed or surrounded by these intermetallic compounds. The SiC nanoparticles may also contribute to the initiation of secondary phases, further complicating the microstructure. The increased intermetallic formation, coupled with a less effective grain refinement due to the high heat and accumulated SiC particles in the SZ (refer to Fig. 8), leads to reduced joint strength [63]. The coarser grain structure and more extensive intermetallic layer at 1600 rpm may account for the observed decrease in joint strength compared to samples welded at 1400 rpm. Excessive IMC formation can lead to cracks and reduced toughness, making the joint more susceptible to failure under mechanical loading.

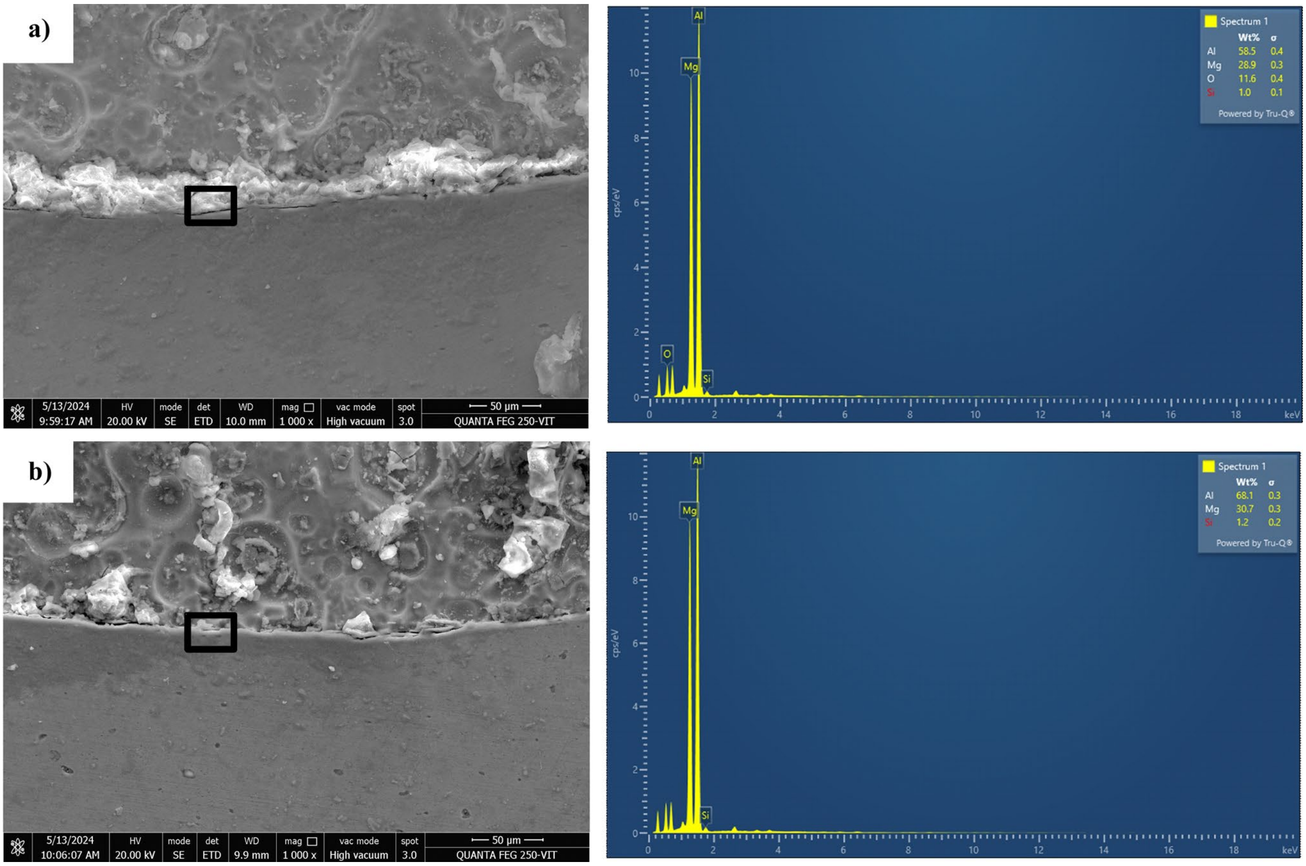

Fig. 6 FESEM at the EDS area scanning analysis at interface locations of Al/Mg **a** 1400 rpm and **b** 1600 rpm

Fig. 7 FESEM Micrograph at SZ of the sample made with tool rotational speed of 1400 rpm

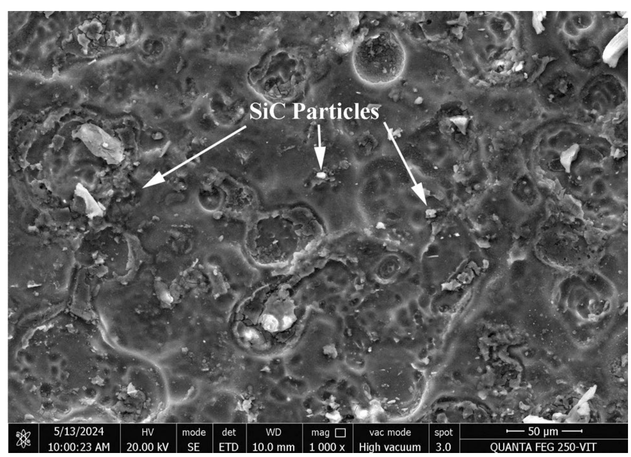

3.2 Tensile shear loads

In this study, lap shear tension tests were employed to study the mechanical properties of the welded samples. Three lap shear tensile tests for each welding condition were conducted according to the ASTM-E08 standard. Figure 9 shows the results of the average lap shear tensile tests for the spot joints by the four different tool rotational speeds and comparison with the particles free spot joints. As the tool rotational speed increased, the lap shear tensile loads of the spot joints initially rise before eventually declining. Figure 9 illustrates that joint incorporating SiC nanoparticles exhibited higher lap shear fracture loads compared to joints without at the same rotational speeds. Specifically,

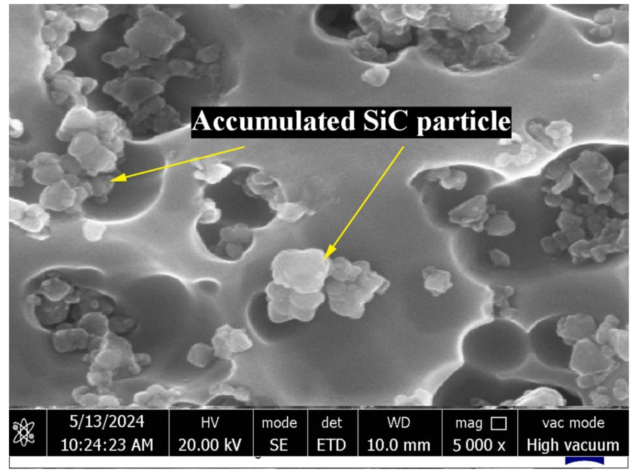

Fig. 8 FESEM Micrograph at SZ of the sample made with tool rotational speed of 1600 rpm

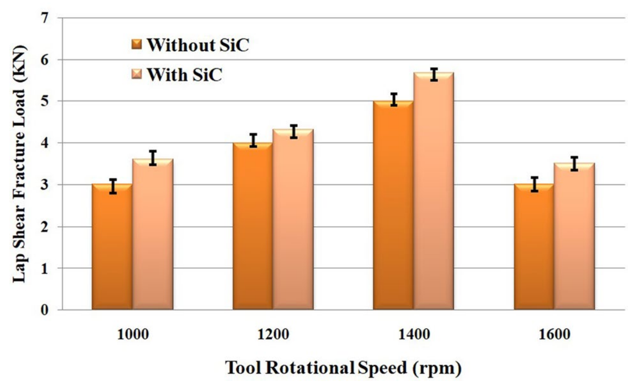

Fig. 9 Lap shear tensile strength of the spot joints by the different tool rotational speed conditions

the lap shear tensile loads for joints with SiC nanoparticles were greater by 3.6 kN, 4.32 kN, 5.68 kN, and 3.5 kN at rotational speeds of 1000 rpm, 1200 rpm, 1400 rpm, and 1600 rpm, respectively. This corresponds to improvements in fracture loads of 20.0%, 10.6%, 22.7%, and 16.6% over the joints without the addition of SiC nanoparticles. The enhanced performance can be attributed to the improved material flow and the changes in IMCs, which significantly contributed to the increased lap shear tensile loads. The peak fracture load of 5.68 kN was achieved at a rotational speed of 1400 rpm. The reduction can be explained by the probable agglomeration of nano-SiC particles in the weld stir zone and the formation of intermetallic compounds such as $Al_{12}Mg_{17}$ and Al_3Mg_2 in the weld zone [64].

Figure 10 provides detailed insights into the fracture surface morphologies of the Al/Mg spot joint with SiC nanoparticles, processed at different rotational speeds. Figure 10a, b illustrate the fracture surfaces at various positions of the joint processed at 1400 rpm. These morphologies exhibit a mix of ductile and brittle fractures, particularly noticeable at the SZ boundary on the Mg side. The presence of numerous dimples of varying sizes indicates a typical ductile fracture mode, which aligns with findings from Tabasi et al. [65] regarding dissimilar friction stir welding of AZ31 to AA7075. In contrast, Fig. 10c, d present the FESEM images of the fracture surfaces of specimens welded at 1600 rpm. The quasi-cleavage fracture patterns observed here are indicative of the brittle behavior of the FSS welded joints, which correlates with a significant reduction in lap shear fracture strength. This comparison underscores the impact of rotational speed on the fracture characteristics and overall joint performance.

4 Conclusion

The FSSW of Al6061-T6 and AZ31B was successfully fabricated by varying tool rotational speed, leading to the following conclusions:

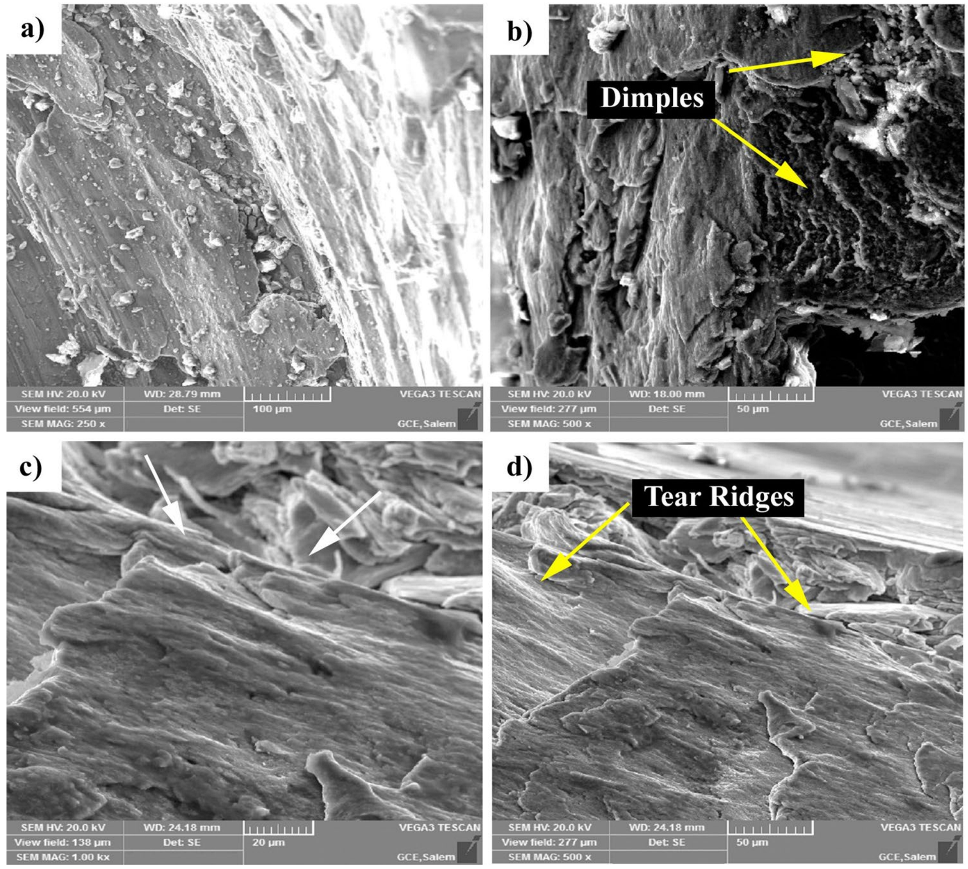

Fig. 10 Typical fracture surfaces of joints at different rotation speeds: **a**, **b** 1400 rpm and **c**, **d** 1600 rpm

- The formation of a fine grain structure in the stir zone (SZ), particularly within the Al–Mg mixing region, demonstrates the effectiveness of the stirring action in achieving thorough material mixing, which is crucial for high joint strength. The incorporation of SiC nanoparticles promotes grain refinement and enhances the overall mechanical properties of the joint.
- SiC nanoparticles improve joint strength by refining the grain structure and limiting intermetallic formation. However, at higher rotational speeds, such as 1600 rpm, excessive heat generation leads to an increase in intermetallic compounds, resulting in more brittle joints with reduced strength.
- At an optimized rotational speed of 1400 rpm, the balance between sufficient material bonding and controlled IMC formation was achieved, resulting in a maximum tensile strength of 5.68 kN. This highlights the importance of process optimization to maximize joint performance.
- Although this study focuses on mechanical strength and grain refinement, future work should explore additional properties such as corrosion resistance, thermal behavior, and fatigue life. These aspects are critical for aerospace applications, where long-term performance and environmental resistance are essential.

Nevertheless, the findings reported in this article demonstrate the potentiality of reinforcing SiC nanoparticles in dissimilar Al/Mg joints, making them more viable for automotive and aerospace applications.

Author contributions Conceptualization, methodology, formal analysis: S.S. and E.N. Writing—original draft preparation: S.S., E.N., and K.M. Review and editing: S.S., G.A., and E.R.

Data availability The authors confirm that the data supporting the findings of this study are available within the article. Raw data that supports the findings of this study are available from the corresponding author, upon reasonable request.

Declarations

Competing interests The authors declare no competing interests.

References

1. Daehn GS. 13—Sustainable design and manufacture of lightweight vehicle structures. In: Folkson R, editor. Alternative fuels and advanced vehicle technologies for improved environmental performance. Woodhead Publishing; 2014. p. 433–61. https://doi.org/10.1533/9780857097422.2.433.
2. Mayyas AT, Mayyas AR, Omar M. 11—Sustainable lightweight vehicle design: a case study in eco-material selection for body-in-white. In: Njuguna J, editor. Lightweight Composite Structures in Transport. Woodhead Publishing; 2016. p. 267–302. https://doi.org/10.1016/B978-1-78242-325-6.00011-6.
3. Mallieswaran K, Rajendran C, Padmanabhan R, Rajasekaran S. Evaluation of nickel shot peening process on strength of friction stir welded AA2014-T6 aluminum alloy joints. Pract Metallogr. 2023;60(7):442–60. https://doi.org/10.1515/pm-2022-1038.
4. Samuel Ratna Kumar PS, Mashinini PM, Vaira Vignesh R. Overview of Lightweight Metallic Materials. In: Vignesh RV, Padmanaban R, Govindaraju M, editors. Advances in processing of lightweight metal alloys and composites: microstructural characterization and property correlation. Singapore: Springer Nature Singapore; 2023. p. 75–87. https://doi.org/10.1007/978-981-19-7146-4_4.
5. Rajendran C, Ben Ruben R, Ashokavarthanan P, Mallieswaran K. Identifying the effect of PWHT on strength of laser beam welding joints of AA2024 aluminum alloy. ASME Open J Eng. 2022. https://doi.org/10.1115/1.4053496.
6. Venkataramanan AR, Dhanenthiran M, Balasubramanian K, Mallieswaran K, Vinosh M. Predict the fatigue life of solution treated and aged TIG welded AA6061 aluminum alloy joints. AIP Conf Proc. 2022. https://doi.org/10.1063/5.0108128.
7. Suresh S, Natarajan E, Vinayagamurthi P, Venkatesan K, Viswanathan R, Rajesh S. Optimum tool traverse speed resulting equiaxed recrystallized grains and high mechanical strength at swept friction stir spot welded AA7075-T6 Lap Joints. In: Natarajan E, Vinodh S, Rajkumar V, editors. Materials, design and manufacturing for sustainable environment. Singapore: Springer Nature Singapore; 2023. p. 547–55. https://doi.org/10.1007/978-981-19-3053-9_41.
8. Zhang W, Xu J. Advanced lightweight materials for automobiles: a review. Mater Des. 2022;221: 110994. https://doi.org/10.1016/j.matdes.2022.110994.
9. Ulutaş A. Joining techniques like welding in lightweight material structures. IGI Global; 2021. p. 121–52. https://doi.org/10.4018/978-1-7998-7864-3.ch006.
10. Balaji J, Seikh AH, Kalam MA, Venkatesh R. Influences of rotational speed on friction stir welding quality, mechanical and fatigue behaviour of AA6061/SiC composite. SILICON. 2024;16(1):323–9. https://doi.org/10.1007/s12633-023-02684-0.
11. Kayode O, Akinlabi ET. An overview on joining of aluminium and magnesium alloys using friction stir welding (FSW) for automotive lightweight applications. Mater Res Expr. 2019;6(11): 112005. https://doi.org/10.1088/2053-1591/ab3262.
12. Gerlich AP. Welding and joining of light alloys. In: Caballero FG, editor. Encyclopedia of materials: metals and alloys. Oxford: Elsevier; 2022. p. 234–44. https://doi.org/10.1016/B978-0-12-819726-4.00063-6.
13. Yang J, et al. Laser techniques for dissimilar joining of aluminum alloys to steels: a critical review. J Mater Process Technol. 2022;301: 117443. https://doi.org/10.1016/j.jmatprotec.2021.117443.
14. Mallieswaran K, Padmanabhan R. Effect of sheet thickness on the FSW parameters for dissimilar aluminium grades tailor welded blanks. Adv Mater Process Technol. 2021;7(1):150–65. https://doi.org/10.1080/2374068X.2020.1754744.
15. Feizollahi V, Yousefi M, Elahifar A, Pourmirza B, Ghobeiti Hasab M, Heidary Moghadam A. Effect of shoulder diameter, tool rotation speed, and arrangement of plates on mechanical and metallurgical properties of dissimilar aluminum 2024–T3 and 7075–T6 friction stir spot welding (FSSW). Eng Fail Anal. 2024;163: 108548. https://doi.org/10.1016/j.engfailanal.2024.108548.
16. Suresh S, Venkatesan K, Natarajan E, Rajesh S, Lim WH. Evaluating weld properties of conventional and swept friction stir spot welded 6061–T6 aluminium alloy. Mater Express. 2019;9(8):851–60. https://doi.org/10.1166/mex.2019.1584.
17. Suresh S, Elango N, Venkatesan K, Lim WH, Palanikumar K, Rajesh S. Sustainable friction stir spot welding of 6061–T6 aluminium alloy using improved non-dominated sorting teaching learning algorithm. J Mater Res Technol. 2020;9(5):11650–74. https://doi.org/10.1016/j.jmrt.2020.08.043.
18. Sasikala G, et al. Optimization of process parameters for friction stir welding of different aluminum alloys AA2618 to AA5086 by Taguchi method. Adv Mater Sci Eng. 2022;2022:1–9. https://doi.org/10.1155/2022/3808605.
19. Sindhuja M, Neelakrishnan S, Davidson BS. Friction stir welding parameters and their influence on mechanical properties of welded AA6061 and AA5052 aluminium plates. Mater Res Expr. 2021;8(10): 106525. https://doi.org/10.1088/2053-1591/ac2daf.
20. Mohammed MM, Abdullah ME, Rohim MNM, Kubit A, Aghajani Derazkola H. AA5754–Al2O3 nanocomposite prepared by friction stir processing: microstructural evolution and mechanical performance. J Manuf Mater Process. 2024. https://doi.org/10.3390/jmmp8020058.

21. Aghajani Derazkola H, Simchi A. Processing and characterizations of polycarbonate/alumina nanocomposites by additive powder fed friction stir processing. Thin Walled Struct. 2020;157: 107086. https://doi.org/10.1016/j.tws.2020.107086.
22. Derazkola HA, Kubit A. Effects of Fe2O3 nanoparticle on quality of medium-density polyethylene friction stir weld joint. Arch Civ Mech Eng. 2024;24(4):228. https://doi.org/10.1007/s43452-024-01039-9.
23. Suresh S, Natarajan E, Mohan DG, Ang CK, Sudhagar S. Depriving friction stir weld defects in dissimilar aluminum lap joints. Proc Inst Mech Eng Part E J Process Mech Eng. 2024. https://doi.org/10.1177/09544089241239817.
24. Palanikumar K, Natarajan E, Suresh S, Mohan DG, Prakash C, Kaur K. Prospects of friction stir processed Mg alloys and composites-Reviews and suggestions. J Mater Res Technol. 2024;31:971–97. https://doi.org/10.1016/j.jmrt.2024.06.087.
25. Ponnusamy V, Muthaiyan R, Subramanian S, Govindasamy R. Silicon carbide nanoparticle-enabled strengthening of aluminum and copper resistance spot welds. Mater Sci. 2024. https://doi.org/10.5755/j02.ms.38335.
26. Derazkola HA, Khodabakhshi F, Gerlich AP. Fabrication of a nanostructured high strength steel tube by friction-forging tubular additive manufacturing (FFTAM) technology. J Manuf Process. 2020;58:724–35. https://doi.org/10.1016/j.jmapro.2020.08.070.
27. Derazkola HA, Khodabakhshi F, Simchi A. Evaluation of a polymer-steel laminated sheet composite structure produced by friction stir additive manufacturing (FSAM) technology. Polym Test. 2020;90: 106690. https://doi.org/10.1016/j.polymertesting.2020.106690.
28. Derazkola HA, Khodabakhshi F. Development of fed friction-stir (FFS) process for dissimilar nanocomposite welding between AA2024 aluminum alloy and polycarbonate (PC). J Manuf Process. 2020;54:262–73. https://doi.org/10.1016/j.jmapro.2020.03.020.
29. Heidarzadeh A, et al. Friction stir welding/processing of metals and alloys: a comprehensive review on microstructural evolution. Prog Mater Sci. 2021;117: 100752. https://doi.org/10.1016/j.pmatsci.2020.100752.
30. Bagheri B, Alizadeh M, Mirsalehi SE, Shamsipur A, Abdollahzadeh A. Nanoparticles addition in AA2024 aluminum/pure copper plate: FSSW approach, microstructure evolution, texture study, and mechanical properties. JOM. 2022;74(11):4420–33. https://doi.org/10.1007/s11837-022-05481-z.
31. Mofid MA, Loryaei E, Heidary MH. Formation of intermetallic compounds at the interface of the friction stir weld and diffusion bond of Mg-AZ31/Al-5083 joint. J Weld Join. 2019;37(6):591–8. https://doi.org/10.5781/JWJ.2019.37.6.9.
32. Zhang MX, Huang H, Spencer K, Shi YN. Nanomechanics of Mg-Al intermetallic compounds. Surf Coatings Technol. 2010. https://doi.org/10.1016/j.surfcoat.2009.11.031.
33. Dong Z, Song Q, Ai X, Lv Z. Effect of joining time on intermetallic compound thickness and mechanical properties of refill friction stir spot welded dissimilar Al/Mg alloys. J Manuf Process. 2019;42:106–12. https://doi.org/10.1016/j.jmapro.2019.04.013.
34. Sarila V, Koneru HP, Cheepu M, Chigilipalli BK, Kantumuchu VC, Shanmugam M. Microstructural and mechanical properties of AZ31B to AA6061 dissimilar joints fabricated by refill friction stir spot welding. J Manuf Mater Process. 2022. https://doi.org/10.3390/jmmp6050095.
35. Chowdhury SH, Chen DL, Bhole SD, Cao X, Wanjara P. Lap shear strength and fatigue behavior of friction stir spot welded dissimilar magnesium-to-aluminum joints with adhesive. Mater Sci Eng A. 2013;562:53–60. https://doi.org/10.1016/j.msea.2012.11.039.
36. Mohammadi J, et al. Friction stir welding joint of dissimilar materials between AZ31B magnesium and 6061 aluminum alloys: Microstructure studies and mechanical characterizations. Mater Charact. 2015;101:189–207. https://doi.org/10.1016/j.matchar.2015.01.008.
37. Wu S, Sun T, Shen Y, Yan Y, Ni R, Liu W. Conventional and swing friction stir spot welding of aluminum alloy to magnesium alloy. Int J Adv Manuf Technol. 2021;116(7):2401–12. https://doi.org/10.1007/s00170-020-06548-4.
38. Aghajani Derazkola H, Simchi A. Effects of alumina nanoparticles on the microstructure, strength and wear resistance of poly(methyl methacrylate)-based nanocomposites prepared by friction stir processing. J Mech Behav Biomed Mater. 2018;79:246–53. https://doi.org/10.1016/j.jmbbm.2018.01.007.
39. Kubit A, Derazkola HA, Myśliwiec P, Szawara P, Slota J, Macek W. Effects of polymer sealant interlayer on quality of EN AW-2024-T3 aluminum alloy lap joint prepared by friction stir welding. Arch Civ Mech Eng. 2024;24(4):238. https://doi.org/10.1007/s43452-024-01047-9.
40. Derazkola HA, Khodabakhshi F. A novel fed friction-stir (FFS) technology for nanocomposite joining. Sci Technol Weld Join. 2020;25(2):89–100. https://doi.org/10.1080/13621718.2019.1631534.
41. Casati R, Vedani M. Metal matrix composites reinforced by nano-particles—a review. Metals (Basel). 2014;4(1):65–83.
42. Sharma V, Prakash U, Kumar BVM. Surface composites by friction stir processing: a review. J Mater Process Technol. 2015;224:117–34. https://doi.org/10.1016/j.jmatprotec.2015.04.019.
43. Suresh S, Natarajan E, Shanmugam R, Venkatesan K, Saravanakumar N, AntoDilip A. Strategized friction stir welded AA6061-T6/SiC composite lap joint suitable for sheet metal applications. J Mater Res Technol. 2022;21:30–9. https://doi.org/10.1016/j.jmrt.2022.09.022.
44. Suresh S, Natarajan E, Franz G, Rajesh S. Differentiation in the SiC filler size effect in the mechanical and tribological properties of friction-spot-welded AA5083-H116 alloy. Fibers. 2022;10(12):109. https://doi.org/10.3390/fib10120109.
45. Suresh S, Venkatesan K, Natarajan E, Rajesh S. Influence of tool rotational speed on the properties of friction stir spot welded AA7075-T6/Al2O3 composite joint. Mater Today Proc. 2020;27:62–7. https://doi.org/10.1016/j.matpr.2019.08.220.
46. Suresh S, Venkatesan K, Rajesh S. Optimization of process parameters for friction stir spot welding of AA6061/Al2O3 by Taguchi method. AIP Conf Proc. 2019. https://doi.org/10.1063/1.5117961.
47. Suresh S, Venkatesan K, Natarajan E. Influence of SiC nanoparticle reinforcement on FSS welded 6061–T6 aluminum alloy. J Nanomater. 2018;2018:1–11. https://doi.org/10.1155/2018/7031867.
48. Suresh S, Venkatesan K, Natarajan E, Rajesh S. Performance analysis of nano silicon carbide reinforced swept friction stir spot weld joint in AA6061-T6 alloy. SILICON. 2021;13(10):3399–412. https://doi.org/10.1007/s12633-020-00751-4.
49. Firouzdor V, Kou S. Al-to-Mg friction stir welding: effect of positions of Al and Mg with respect to the welding tool. Weld J (Miami, Fla). 2009;88:213S-224S.
50. Yang Y, Paidar M, Mehrez S, Ojo OO. Enhancement of mechanical properties and wear of AA5083/316 stainless steel surface-composite developed through multi-pass friction stir processing (MPFSP). Arch Civ Mech Eng. 2022;23(1):13. https://doi.org/10.1007/s43452-022-00556-9.
51. Memon S, Paidar M, Mehrez S, Cooke K, Ojo OO, Lankarani HM. Effects of materials positioning and tool rotational speed on metallurgical and mechanical properties of dissimilar modified friction stir clinching of AA5754-O and AA2024-T3 sheets. Results Phys. 2021;22: 103962. https://doi.org/10.1016/j.rinp.2021.103962.

52. Liu S, Paidar M, Mehrez S, Ojo OO, Mahariq I, Elbadawy I. Development of AA6061/316 stainless steel surface composites via friction stir processing: Effect of tool rotational speed. Mater Charact. 2022;192: 112215. https://doi.org/10.1016/j.matchar.2022.112215.
53. Fan G, et al. Positional variation of AA5083-H112 and AA6061-T6 alloys: Modified friction stir clinching. Vacuum. 2022;196: 110712. https://doi.org/10.1016/j.vacuum.2021.110712.
54. Li J, Tang F, Paidar M. Modified friction stir clinching-brazing of brass to AA5083 aluminum alloy using Zn interlayer. Arch Civ Mech Eng. 2021;21(1):13. https://doi.org/10.1007/s43452-020-00162-7.
55. Fu B, Qin G, Li F, Meng X, Zhang J, Wu C. Friction stir welding process of dissimilar metals of 6061–T6 aluminum alloy to AZ31B magnesium alloy. J Mater Process Technol. 2015;218:38–47. https://doi.org/10.1016/j.jmatprotec.2014.11.039.
56. Suresh S, Velmurugan D, Balaji J, Natarajan E, Suresh P, Rajesh S. Influences of nanoparticles in friction stir welding processes. In: Sustainable utilization of nanoparticles and nanofluids in engineering applications. IGI Global; 2023. p. 32–55. https://doi.org/10.4018/978-1-6684-9135-5.ch002.
57. Natrayan L, et al. Enhancement of mechanical properties on novel friction stir welded Al-Mg-Zn alloy joints reinforced with nano-SiC particles. J Nanomater. 2021;2021:1–10. https://doi.org/10.1155/2021/2555525.
58. Zou Y, et al. The influence of tool shape on the microstructure evolution and tribological properties during friction stir processing of AlCoCrFeNi high entropy alloys particle reinforced AA7075 aluminum alloy. Vacuum. 2024;229: 113540. https://doi.org/10.1016/j.vacuum.2024.113540.
59. Men J, et al. Investigation on microstructure, mechanical and tribological properties of friction stir processing of AZ31/AlFeCrMoNb surface composite. Mater Chem Phys. 2024;317: 129149. https://doi.org/10.1016/j.matchemphys.2024.129149.
60. Acharya U, Kumar U, Ghosh M, Choudhury S, Srivastava AK, Roy BS. An experimental approach for achieving high strength dissimilar aluminium-magnesium joints: application of tool pin profiles on different joint configurations. CIRP J Manuf Sci Technol. 2023;45:49–60. https://doi.org/10.1016/j.cirpj.2023.06.003.
61. Choudhury S, Das R, Sethi D, Roy J, Roy BS. Critical assessment 43: microstructural and mechanical properties of friction stir additively fabricated SiC-Reinforced AA6061 build. Mater Sci Technol. 2023;39(18):3090–110. https://doi.org/10.1080/02670836.2023.2239634.
62. Esposito A. (PC) for robotics and automation. p. 46–80.
63. Shah LH, Othman NH, Gerlich A. Review of research progress on aluminium–magnesium dissimilar friction stir welding. Sci Technol Weld Join. 2018;23(3):256–70. https://doi.org/10.1080/13621718.2017.1370193.
64. Chen B, Wang Y, Xiao C, Zhang M, Ni G, Li D. The formation mechanism of intermetallic compounds in Al/Mg friction-stir weld joint. Mater Sci Technol. 2018;34(6):703–11. https://doi.org/10.1080/02670836.2017.1410926.
65. Tabasi M, Farahani M, Givi MKB, Farzami M, Moharami A. Dissimilar friction stir welding of 7075 aluminum alloy to AZ31 magnesium alloy using SiC nanoparticles. Int J Adv Manuf Technol. 2016;86(1–4):705–15. https://doi.org/10.1007/s00170-015-8211-y.